RESEARCH ARTICLE
doi: 10.2306/scienceasia1513-1874.2025.s028

ScienceAsia 51S (2): 2025: ID 2025s028: **1–8**

High-performance mid-infrared supercontinuum generation in all-anomalous-dispersion $AsSe_2$-As_2S_5 chalcogenide hybrid microstructured optical fibers

Amphon Lukboon[a,b], Panatcha Anusasananan[a], Mongkol Wannaprapa[c], Suksan Suwanarat[a,*]

[a] Department of Physics, Faculty of Science, Ramkhamhaeng University, Bangkok 10240 Thailand
[b] Valaya Alongkorn Rajabhat University Demonstration School, Valaya Alongkorn Rajabhat University, Pathum Thani 13180 Thailand
[c] Department of Electronics Technology, Faculty of Science, Ramkhamhaeng University, Bangkok 10240 Thailand

*Corresponding author, e-mail: suksan@ru.ac.th

Received 19 Nov 2024, Accepted 29 Nov 2025
Available online 20 Dec 2025

ABSTRACT: Mid-infrared (Mid-IR) supercontinuum (SC) generation with a large optical bandwidth and an easily fabricated device is poised to become an enabling technology for Mid-IR SC devices. In this work, we numerically demonstrate Mid-IR SC generation in all-anomalous dispersion $AsSe_2$-As_2S_5 chalcogenide (ChG) hybrid microstructured optical fibers (HMOFs). To achieve Mid-IR SC spectra extending beyond 10 μm, As_2S_5 and $AsSe_2$ ChG materials were considered, owing to their high transparency in this spectral range. The optimized fiber, consisting of an $AsSe_2$ core (radius $r = 1.9$ μm) and an As_2S_5 cladding (radius $R = 4.4$ μm), exhibits all-anomalous dispersion with small magnitudes ranging from +4.08 ps/nm/km to +49.78 ps/nm/km over the wavelength range from∼3.2 μm to 10 μm and supports a well-confined fundamental TE mode (horizontally polarized), using a two-dimensional finite-difference eigenmode solver. Numerical simulations performed using the split-step Fourier method show that, when pumped with 200-fs pulses and a peak power of 3000 W at a wavelength 3.4 μm, the 4.0-mm-long $AsSe_2$-As_2S_5 HMOFs can generate SC spectra spanning from 1.7 μm to 9.3 μm (−40 dB bandwidth of 7600 nm). By increasing the pulse duration to 300 fs and using the same pump source, the 5.8-mm-long fiber achieves an even broader spectrum, covering 1.7 μm to 10.2 μm. The nonlinear broadening mechanisms are dominated by self-phase modulation and four-wave mixing. The demonstrated high-performance Mid-IR SC generation—combining ultra-broadband operation, compact structure, and low-energy (< 1 pJ) pulse requirements—shows strong potential for enabling novel on-chip Mid-IR SC device architectures.

KEYWORDS: supercontinuum generation, anomalous dispersion, chalcogenide optical fiber, self-phase modulation, four-wave mixing

INTRODUCTION

Supercontinuum (SC) generation in the mid-infrared (Mid-IR) regime has attracted considerable attention owing to its wide range of applications, including biomedical imaging, high-precision measurements, optical tomography, and spectroscopy [1, 2]. Due to its extremely broad wavelength coverage in the Mid-IR region, SC generation is often employed as a light source for these applications. Mid-IR SC spectra extending toward longer wavelengths are of particular interest for nondestructive reflectance imaging of biological tissues *in vivo*. Petersen et al [3] reported a Mid-IR SC source spanning 2 μm to 7.5 μm in a ZrF_2–BaF_2–LaF_3–AlF_3–NaF chalcogenide glass (ChG) fiber for Mid-IR multispectral tissue imaging at selected wavelengths between 5.7 μm and 7.3 μm, which could complement current cancer diagnostic methods. SC generation arises from continuous spectral broadening during the propagation of high-power ultrashort pulses through a nonlinear medium. Optical waveguides and fibers play a key role in this process. Both structures consist of a central glass core surrounded by a cladding layer with a lower refractive index. Their relatively high refractive index contrast allows light to be confined within a small core area, enhancing nonlinear effects when the dispersion is engineered near the pump wavelength. The materials used in waveguides and fibers must provide transparency over a wide wavelength range. The SC process depends strongly on material dispersion, and the dispersion can be tailored and optimized by adjusting the geometries of the waveguides and fibers. To extend the SC bandwidth, the pump wavelength is typically chosen far from the zero-dispersion wavelength (ZDW) in the anomalous dispersion regime ($D > 0$) to enhance nonlinear effects [1–7]. Recently, several theoretical and experimental demonstrations of Mid-IR SC generation have been reported in ChG waveguides and microstructured optical fibers (MOFs). For waveguides operating in the anomalous dispersion regime, Lamont et al [4] reported a 60-mm-long As_2S_3 planar waveguide generating SC spectra from 1.2 μm to 2 μm, using 610-fs pulses with a peak power of 68 W at a wavelength of 1.55 μm. Bunyasit et al [8] reported a 1-mm-long As_2S_5 ridge waveguide generating SC spectra spanning 1.25 μm to 13 μm, using 50-fs pulses with a peak power of 2.0 kW at a wavelength of 2.5 μm. For fibers operating in the anomalous dispersion regime,

Hudson et al [9] reported a 72-mm-long As_2S_3 fiber generating SC spectra from 1.6 µm to 5.9 µm, using 67-fs pulses with a peak power of 520 kW at a wavelength of 3.1 µm. Gao et al [10] demonstrated a 4.8-cm-long four-hole As_2S_5 HMOF, fabricated using the rod-in-tube method, which generated SC spectra extending from 1.37 µm to 5.65 µm when pumped with a 1.5-kW peak power at a wavelength of 2.3 µm. Møller et al [11] reported an 18-cm-long $As_{38}S_{62}$ MOF generating SC spectra spanning 1.7 µm to 7.5 µm, using 320-fs pulses with a peak power of 5.2 kW at a wavelength of 4.4 µm. Wang et al [12] reported an As_2S_5 fiber producing broadband SC spectra from 1.03 µm to 3.44 µm, using 200-fs pulses at a wavelength of 2 µm. Qu et al [13] reported an 11-mm-long $AsSe_2$-As_2S_5 MOF generating broadband SC spectra extending from 1.3 µm to 11 µm, using 100-fs pulses with a peak power of 20 kW at a wavelength of 6 µm. Waveguide fabrication typically involves complex processes such as thermal evaporation, plasma reactive ion etching using CHF_3 gas, and subsequent coating [4]. In contrast, fibers are generally fabricated using the rod-in-tube drawing method [14–17], which is simpler and more cost-effective. Therefore, developing Mid-IR SC generation with a broad optical bandwidth and a structure that is easy to fabricate has become a goal with significant scientific and industrial interest.

To achieve SC generation with a broad optical bandwidth extending beyond 10 µm using a simple, single-fiber structure suitable for practical fabrication via the rod-in-tube technique, dispersion engineering plays a crucial role. Ideally, the fiber should exhibit anomalous dispersion ($D > 0$) near the pump wavelength, with a small and nearly constant dispersion value across the operating range [1–7]. In a previous work, Cheng et al [15] experimentally demonstrated a 2-cm-long four-hole $AsSe_2$-As_2S_5 HMOF producing SC spectra from approximately 1.26 µm to 5.4 µm when pumped with 200-fs pulses at a wavelength of $\sim$ 3.39 µm and a peak power of 1337 kW. The As_2S_5 and $AsSe_2$ ChG materials offer significant potential for extending SC generation, owing to their broad transparency window in the Mid-IR spectral range of $\sim$ 0.6 µm to 12 µm and stable transmission of about 65% [14–22]. To demonstrate the practical feasibility of Mid-IR SC devices, the As_2S_5 and $AsSe_2$ materials and the 200-fs pump pulse at a wavelength of 3.4 µm used in this study are based on the parameters reported by Cheng et al [15].

In this paper, we numerically demonstrate that $AsSe_2$-As_2S_5 ChG HMOFs in the anomalous dispersion can generate SC spectra in the Mid-IR range extending beyond 10 µm. The proposed fiber consists of an $AsSe_2$ core (radius r) and an As_2S_5 cladding (radius R), with refractive indices of 2.83 and 2.24, respectively, at a wavelength of 3.4 µm, providing an index contrast of 0.59. The dispersion-engineered $AsSe_2$-As_2S_5 HMOFs are designed using a two-dimensional (2D) finite-difference eigenmode (FDE) solver [23–26] to exhibit all-anomalous dispersion with a small magnitude and to support the fundamental TE mode over the Mid-IR range. Simulation results include the propagation constant ($\beta(\omega)$) over a frequency range and the effective mode area (A_{eff}) at the pump wavelength. The $\beta(\omega)$ is used to calculate the effective mode index (n_{eff}), as well as the group-velocity dispersion (GVD) parameter and higher-order dispersion parameters [1–7]. To study SC generation, a femtosecond soliton pulse is launched into the $AsSe_2$-As_2S_5 HMOF, exciting the fundamental TE mode and propagating as a high-order soliton. The optimized $AsSe_2$-As_2S_5 HMOF is designed to exhibit all-anomalous dispersion and to support SC spectra in the Mid-IR range from 2 µm to 10 µm. The nonlinear evolution of SC generation is simulated by solving the generalized nonlinear Schrödinger equation (GNLSE), using the split-step Fourier method (SSFM) [1–7, 27, 28] with the obtained parameters. The influence of peak power and pulse duration on SC generation is investigated. Simulation results show that a 4.0-mm-long $AsSe_2$-As_2S_5 HMOF with $R = 4.4$ µm and $r = 1.9$ µm can generate the widest Mid-IR SC spectra from 1.7 µm to 9.3 µm, corresponding to a −40 dB bandwidth of 7600 nm. Furthermore, by increasing the pulse duration to 300 fs and using the same pump source, the SC spectra at a fiber length of 5.8 mm can be extended from 1.7 µm to 10.2 µm, with a −40 dB bandwidth of 8500 nm. The dominant nonlinear processes contributing to SC generation are self-phase modulation (SPM) and four-wave mixing (FWM). With its ultra-broadband Mid-IR SC generation, compact structure, and low-energy (< 1 pJ) pulse requirement, this work presents a promising approach for practical Mid-IR SC source development and manufacturing applications.

NUMERICAL SUPERCONTINUUM GENERATION MODELING

Optical fibers consist of a central glass core surrounded by a cladding layer with a lower refractive index. Their relatively high refractive index contrast allows the fiber to confine light within a small core area, thereby enhancing nonlinear effects when the dispersion is engineered near the pump wavelength. The schematic diagram of the $AsSe_2$-As_2S_5 ChG HMOF, based on a simple single-mode fiber structure, is shown in the inset of Fig. 1(a). The design employs $AsSe_2$ ChG as the core with radius r and As_2S_5 ChG as the cladding with radius R. The dispersion characteristics of the optical fiber play a crucial role in broadening the SC spectrum. The wavelength-dependent dispersion is highly sensitive to both the core and cladding dimensions. The fiber dispersion for optical modes can be engineered by varying these dimensions using a 2D FDE solver. This computation yields the $\beta(\omega)$ over a range of frequencies

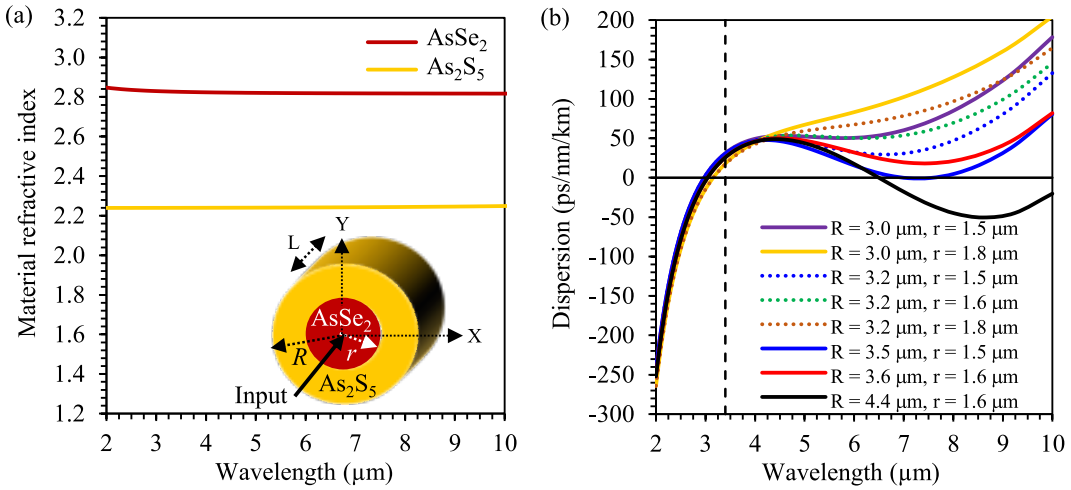

Fig. 1 (Color curves) (a) Linear material refractive indices of $AsSe_2$ and As_2S_5 ChGs and fiber geometry shown in the inset with an $AsSe_2$ core radius r and As_2S_5 cladding radius R for an $AsSe_2$-As_2S_5 ChG HMOF. (b) Calculated dispersion curves of the $AsSe_2$-As_2S_5 ChG HMOFs for the fundamental TE mode, with varying core and cladding dimensions. The vertical dashed line indicates a pump wavelength of 3.4 μm.

and the $A_{\text{eff}} = \left|\int (E\times H^*)\cdot\hat{z}\,\mathrm{d}A\right|^2 / \int |(E\times H^*)\cdot\hat{z}|^2\,\mathrm{d}A$ at the pump wavelength. The effective mode index, $n_{\text{eff}} = \lambda\beta(\omega)/2\pi$, and the GVD parameter, $D(\lambda) = -(\lambda/c)(\mathrm{d}^2 n_{\text{eff}}/\mathrm{d}\lambda^2)$ (ps/nm/km), are subsequently calculated. The propagation constant can be expanded as a Taylor series around the central angular frequency ω_0, expressed as $\beta(\omega) = \beta_0 + \beta_1(\omega-\omega_0)/1! + \beta_2(\omega-\omega_0)^2/2! + \beta_3(\omega-\omega_0)^3/3! + \cdots$, where the higher-order dispersion parameters are $\beta_m = \mathrm{d}^m\beta/\mathrm{d}\omega^m$, with m-th representing the order dispersion parameter [1–7].

To study SC generation, a femtosecond pulse is launched into the $AsSe_2$-As_2S_5 ChG HMOF, where it evolves as a high-order soliton during propagation. The pulse evolution is governed by the GNLSE for the slowly varying envelope $A(z,T)$ [1–7]:

$$\frac{\partial A(z,T)}{\partial z} = -\frac{\alpha}{2}A(z,T) + \mathrm{i}\sum_{m\geqslant 2}^{\infty}\frac{\mathrm{i}^m\beta_m}{m!}\frac{\partial^m A(z,T)}{\partial T^m} + \mathrm{i}\left(\gamma + \frac{\mathrm{i}\alpha_2}{2A_{\text{eff}}}\right)\left(1+\frac{\mathrm{i}}{\omega_0}\frac{\partial}{\partial T}\right)\left(A(z,T)\int_{-\infty}^{\infty}R(T')\left|A(z,T-T')\right|^2\mathrm{d}T'\right) \quad (1)$$

Here, $A(z,T)$ is the electric field envelope; $T = t - z/v_g$ is the retarded time frame moving with the group velocity $v_g = 1/\beta_1(\omega_0)$ at the pump frequency ω_0; $\alpha(\omega)$ is the linear propagation loss; $\beta_m = \mathrm{d}^m\beta/\mathrm{d}\omega^m$ is the m-th-order dispersion parameter; $\gamma = n_2\omega_0/(cA_{\text{eff}})$ is the nonlinear coefficient parameter, where n_2 is the nonlinear refractive index; and α_2 is the two-photon absorption coefficient. The input soliton pulse is defined as $A(0,T) = \sqrt{P_0}\,\mathrm{sech}(T/T_0)$, where P_0 is the peak power; T_0 ($= T_{\text{FWHM}}/1.76$) is the pulse duration; and T_{FWHM} is the pulse full width at the half-maximum (FWHM) of the input. The soliton propagation into the fiber is excited in the form of an N-th-order soliton, $N^2 = L_{\text{D}}/L_{\text{NL}} = \gamma P_0 T_0^2/\beta_2$, where $L_{\text{D}} = T_0^2/\beta_2$ is the dispersion length and $L_{\text{NL}} = (\gamma P_0)^{-1}$ is the nonlinear length. The pulse evolution inside the fiber exhibits nonlinear behavior, and soliton fission occurs at the fission length $L_{\text{fiss}} = L_{\text{D}}/N$ [1–7].

The nonlinear Raman response function $R(t)$ consists of an instantaneous electronic (Kerr) response $\delta(t)$ and a delayed Raman response $h_R(t)$, given by:

$$R(t) = (1-f_R)\delta(t) + f_R h_R(t) \quad (2)$$

$$h_R(t) = \frac{(\tau_1^2+\tau_2^2)}{(\tau_1\tau_2^2)}\,\mathrm{e}^{(-t/\tau_2)}\sin(-t/\tau_1) \quad (3)$$

where the f_R represents the fractional contribution of the delayed Raman response. The simulated parameters for the $AsSe_2$ ChG are $f_R = 0.148$, $\tau_1 = 15.35$ fs, and $\tau_2 = 106.1$ fs [20–22].

The numerical solution to the GNLSE using the SSFM is obtained by taking the Fourier transform of Eq. (1), and with the notation $\tilde{A}(z,\omega) = F[A(z,t)]$ [1–7, 27, 28], given by

$$\frac{\partial\tilde{A}(z,\omega)}{\partial z} = -\frac{\alpha}{2}\tilde{A}(z,\omega) + F\left[\mathrm{i}\sum_{m\geqslant 2}^{\infty}\frac{\mathrm{i}^m\beta_m}{m!}\frac{\partial^m A(z,T)}{\partial T^m}\right] + F\left[\mathrm{i}\gamma(\omega_0)\left(1+\frac{\mathrm{i}}{\omega_0}\frac{\partial}{\partial T}\right)A(z,T)\int_{-\infty}^{\infty}R(T')\left|A(z,T-T')\right|^2\mathrm{d}T'\right] \quad (4)$$

The dispersion to all orders can be expressed in the frequency domain as

$$F\left[\mathrm{i}\sum_{m\geqslant 2}^{\infty}\frac{\mathrm{i}^m\beta_m}{m!}\frac{\partial^m A(z,T)}{\partial T^m}\right] = [\beta(\omega) - \beta(\omega_0) - \beta_1(\omega_0)(\omega-\omega_0)]\tilde{A}(z,\omega) \quad (5)$$

where $\beta(\omega) = n_{\text{eff}}(\omega)\omega/c$, $\beta_1 = \partial\beta/\partial\omega$, and F is the Fourier transform operator.

The linear part of Eq. (4) is defined as

$$\hat{L} = \mathrm{i}\frac{\alpha(\omega)}{2} + \sum_{m\geqslant 2}^{\infty} \beta_m \frac{(\omega-\omega_0)^m}{m!} \tag{6}$$

and the GNLSE in the frequency domain can be rewritten as

$$\frac{\partial \tilde{A}(z,\omega)}{\partial z} = \mathrm{i}\hat{L}\tilde{A}(z,\omega) + F\left[\mathrm{i}\gamma(\omega_0)\left(1+\frac{\mathrm{i}}{\omega_0}\frac{\partial}{\partial T}\right)A(z,T)\int_{-\infty}^{\infty} R(T)\left|A(z,T-T')\right|^2 \mathrm{d}T'\right] \tag{7}$$

Taking $\mathrm{e}^{-\mathrm{i}\hat{L}z}$, Eq. (7) can be rewritten as

$$\left[\frac{\partial \tilde{A}(z,\omega)}{\partial z} - \mathrm{i}\hat{L}\tilde{A}(z,\omega)\right]\mathrm{e}^{-\mathrm{i}\hat{L}z} = \mathrm{e}^{-\mathrm{i}\hat{L}z} F\left[\mathrm{i}\gamma(\omega_0)\left(1+\frac{\mathrm{i}}{\omega_0}\frac{\partial}{\partial T}\right)A(z,T) \times \int_{-\infty}^{\infty} R(T)\left|A(z,T-T')\right|^2 \mathrm{d}T'\right] \tag{8}$$

By changing the variable as follows: $\tilde{A} = \tilde{A}(z,\omega)\,\mathrm{e}^{-\mathrm{i}\hat{L}z}$, the first term is eliminated and the equation to be solved becomes

$$\frac{\partial \tilde{A}}{\partial z} = \mathrm{e}^{-\mathrm{i}\hat{L}z} F\left[\mathrm{i}\gamma(\omega_0)\left(1+\frac{\mathrm{i}}{\omega_0}\frac{\partial}{\partial T}\right)A(z,T) \times \int_{-\infty}^{\infty} R(T)\left|A(z,T-T')\right|^2 \mathrm{d}T'\right] \tag{9}$$

The algorithm for solving the pulse evolution governed by Eq. (1) can be summarized as follows: Step 1: Compute the right-hand side of Eq. (9). Step 2: Propagate the pulse over one step, Δz, by solving in the Fourier domain. MATLAB's built-in 'ode45' solver, which implements the fourth-order Runge-Kutta method, is employed to obtain the updated field. Step 3: Save the resulting field and transform it back into the time domain by performing the inverse Fourier transform. Step 4: Repeat the process iteratively from Step 1 until the desired propagation length is achieved. At the end of the simulation, the stored field values are retrieved, and the results are analyzed in both the time and spectral domains. The MATLAB source code for simulating pulse propagation and supercontinuum generation in optical fibers is available in [27].

RESULTS AND DISCUSSION

The designed $AsSe_2$-As_2S_5 ChG HMOF is illustrated in the inset of Fig. 1(a). The figure shows the wavelength-dependent linear refractive indices of the $AsSe_2$ and As_2S_5 ChG over a wide wavelength range, represented by the solid color curves. The fitted curves were obtained using the Sellmeier equation with fitting coefficients listed in Table 1, where λ is the wavelength in micrometers. The dispersion of the $AsSe_2$-As_2S_5 ChG HMOFs was calculated by varying the core and cladding dimensions, as shown in Fig. 1(b). It can be observed that the material dispersion of $R = 4.4$ µm and $r = 1.6$ µm (solid black curve) remains normal within the wavelength range from 6.7 µm to 10 µm. When the core radius is reduced to $r = 1.8$, 1.6, and 1.5 µm, while fixing $R = 3.2$ µm (dashed curves), the dispersions over the wavelength range from 4.5 µm to 10 µm increased in the anomalous-dispersion region. Similarly, by reducing the radius to $R = 4.4$ µm (solid black curve), 3.6 µm (solid red curve), and 3.2 µm (green dashed curve), while fixing $r = 1.6$ µm, as well as by varying $R = 3.5$ µm (solid blue curve), 3.2 µm (blue dashed curve), and 3.0 µm (solid purple curve) with $r = 1.5$ µm, the dispersions become larger in the anomalous dispersion over the wavelength range from 4.5 µm to 10 µm. These results demonstrate that the dispersion-engineered $AsSe_2$-As_2S_5 ChG HMOFs can be designed to exhibit all-anomalous dispersion with a small magnitude across the wavelength range from $\sim$ 3.2 µm to $>$ 10 µm, enabling efficient mode confinement and supporting Mid-IR SC generation.

Table 1 The Sellmeier fitting coefficients of $AsSe_2$ and As_2S_5 ChGs [14, 15].

$$n^2(\lambda) = 1 + \sum_{j=1}^{m} \frac{B_j \lambda_2^2}{\lambda^2 - \lambda_j^2}$$

Material	As_2S_5		$AsSe_2$	
m	B_j	λ_j^2 (µm^2)	B_j	λ_j^2 (µm^2)
$j=1$	2.1361	0.0954	6.7510	0.1034
$j=2$	0.0693	225.0001	0	153.7990
$j=3$	1.7637	2.1783×10^{-7}	0.1768	1×10^{-32}

As mentioned earlier, the $AsSe_2$-As_2S_5 ChG HMOFs, based on a relatively simple architecture, can be designed to exhibit all-anomalous dispersion over the entire wavelength range, allowing the resulting Mid-IR SC generation to extend across its entre bandwidth. The As_2S_5 and $AsSe_2$ ChG materials are considered because of their excellent transparency in the Mid-IR region, high nonlinear refractive index ($n_2 = 1.1 \times 10^{-17}$ m^2/W), and negligible two-photon absorption in this spectral range [14–22]. To achieve all-anomalous dispersion with a small and nearly constant value over the entire wavelength range, and with the ZDW close to the pump wavelength, a 2D FDE solver was employed by varying the core and cladding dimensions. Fig. 2(a) shows the optimized GVD curves of three $AsSe_2$-As_2S_5 ChG HMOFs with $R = 4.4$ µm, $r = 1.9$ µm; $R = 4.4$ µm, $r = 2.0$ µm; and $R = 4.4$ µm, $r = 2.1$ µm, for the fundamental TE mode at the pump wavelength. It can be observed from Fig. 2(a) that the material dispersions, shown by the solid color curves, exhibit all-anomalous dispersion with small magnitudes across the wavelength range from $\sim$ 3.2 µm to $>$ 10 µm, with ZDWs of $\sim$ 3.3 µm. The corresponding effective area changes only slightly over this range, as shown in

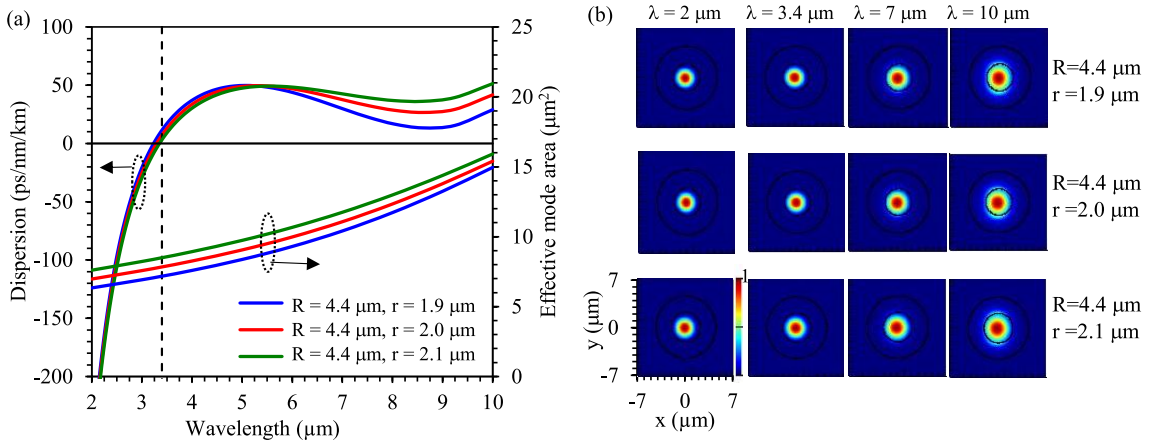

Fig. 2 (a) Calculated dispersion and effective mode area of the three $AsSe_2$-As_2S_5 ChG HMOFs in all-anomalous dispersion, with fixing $R = 4.4$ μm and varying $r = 1.9$, 2.0, and 2.1 μm for the fundamental TE mode, at a pump wavelength of 3.4 μm, and (b) their corresponding mode profiles at different wavelengths of 2, 3.4, 7, and 10 μm. The vertical dashed line indicates the pump wavelength.

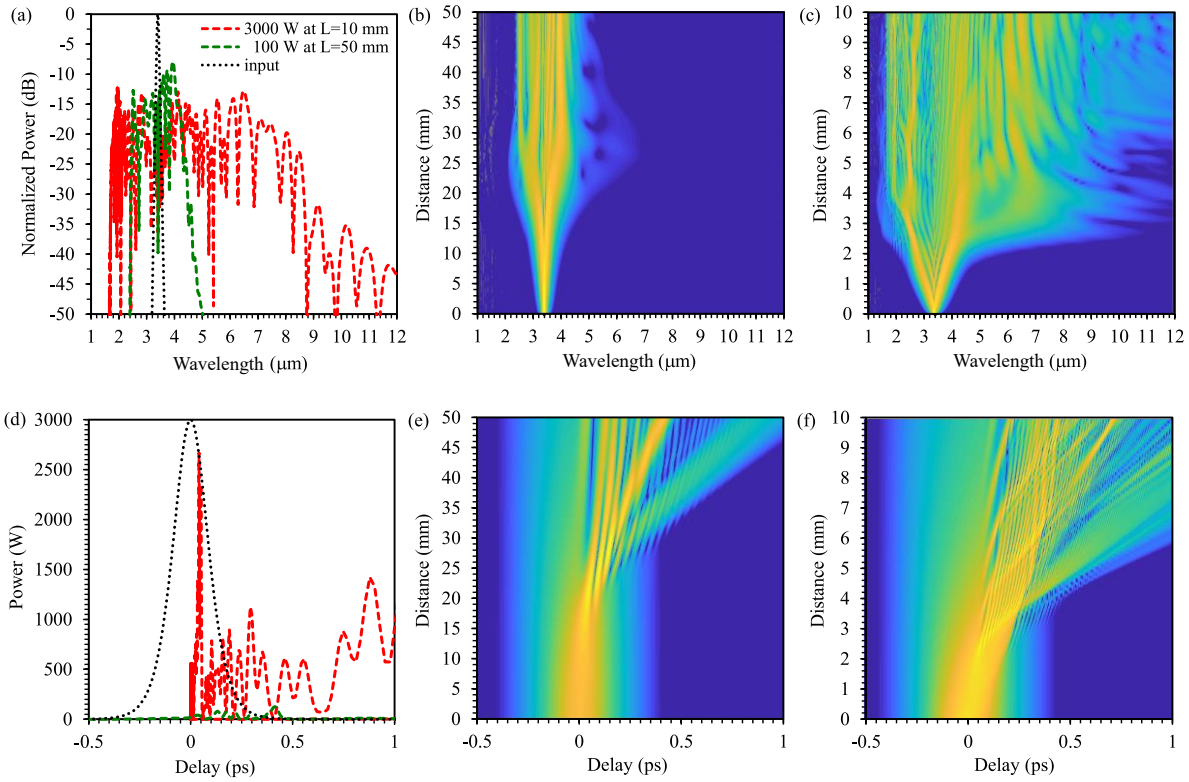

Fig. 3 (Color curves) (a) Spectral and (d) temporal SC profiles with two different peak powers of 100 W and 3000 W at the 10-mm and 50-mm length for the $AsSe_2$-As_2S_5 ChG HMOF in all-anomalous dispersion, with $R = 4.4$ μm and $r = 1.9$ μm, using 200-fs pulses at a pump wavelength of 3.4 μm: (b) and (c) their spectral evolutions, and (e) and (f) their temporal evolutions along the fiber length with two different peak powers of 100 W and 3000 W, respectively. The dotted curves show the input profiles for comparison.

Fig. 2(a). At the pump wavelength, the effective areas of these fibers are $A_{\text{eff}} = 7.176$, 7.832, and 8.449 μm^2, corresponding to the calculated nonlinear coefficients of $\gamma = 2.833$, 2.596, and 2.406 W/m, respectively. Fig. 2(b) presents the optical mode profile at different wavelengths of 2, 3.4, 7, and 10 μm for the funda-

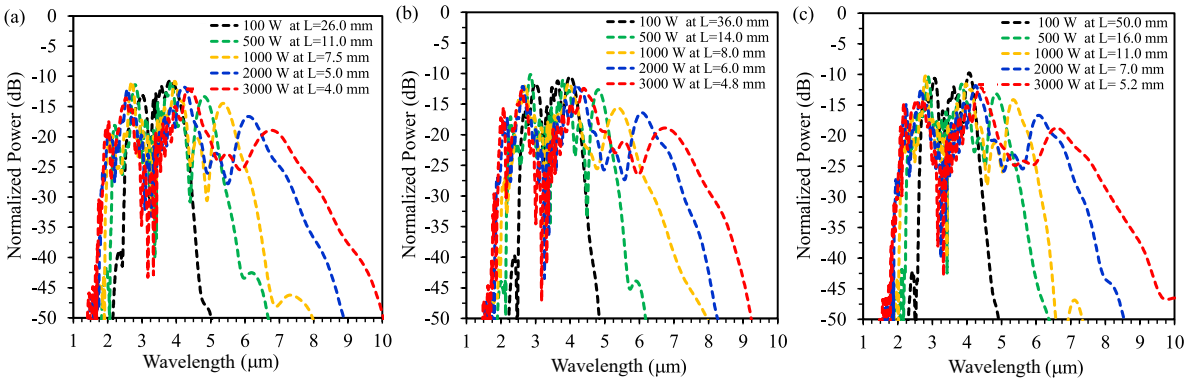

Fig. 4 (Color curves) The widest spectral SC generation with the different peak powers of 100, 500, 1000, 2000, and 3000 W, pumped at a pump wavelength of 3.4 μm using 200-fs pulses for the three $AsSe_2$-As_2S_5 ChG HMOFs in the anomalous dispersion of (a) $R = 4.4$ μm and $r = 1.9$ μm, (b) $R = 4.4$ μm and $r = 2.0$ μm, and (c) $R = 4.4$ μm and $r = 2.1$ μm.

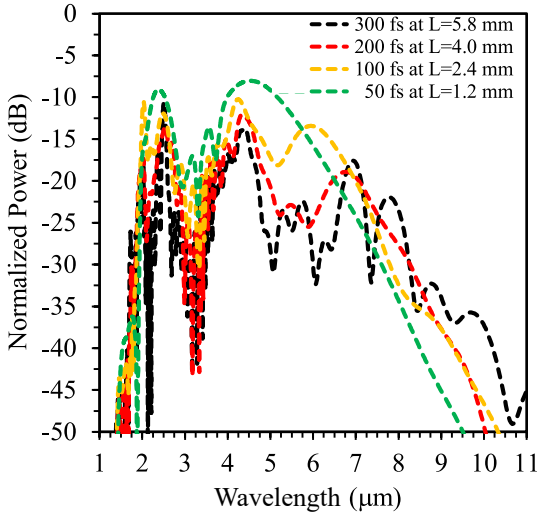

Fig. 5 (Color curves) The widest spectral SC generation with different pulse durations of $T_{FWHM} = 50$, 100, 200, and 300 fs, with a peak power of 3000 W at a pump wavelength of 3.4 μm for the $AsSe_2$-As_2S_5 ChG HMOFs with $R = 4.4$ μm and $r = 1.9$ μm.

mental TE mode. The results show that these fibers can support both the fundamental TE (horizontally polarized) and TM (vertically polarized) modes, with very low confinement loss over the entire wavelength range, owing to their symmetrical structure. The GVD parameter, corresponding to the second-order dispersion, is given by $\beta_2 = \mathrm{d}^2\beta/\mathrm{d}\omega^2 = -(\lambda^2/2\pi c)D(\lambda)$, while the third-order dispersion is defined as $\beta_3 = \mathrm{d}^2\beta_2/\mathrm{d}\omega^2$. The simulated dispersion parameters of the three fibers are $\beta_2 = -6.54818 \times 10^{-2}$ ps^2/m, -3.87458×10^{-2} ps^2/m, and -1.41077×10^{-2} ps^2/m, as well as $\beta_3 = +2.48388 \times 10^{-3}$ ps^3/m, $+2.44285 \times 10^{-3}$ ps^3/m, and $+2.39111 \times 10^{-3}$ ps^3/m, respectively, for the fundamental TE mode at a pump wavelength of 3.4 μm.

We considered a pulse duration of 200 fs at a pump wavelength of 3.4 μm, with peak power ranging from 100 W to 3000 W and a propagation loss of $\alpha = 1.2$ dB/m. Based on our simulation results, Fig. 3(a) and (d) show the spectral and temporal SC profiles in the $AsSe_2$-As_2S_5 ChG HMOF, with $R = 4.4$ μm and $r = 1.9$ for two different peak powers of 100 W and 3000 W. The obtained SC spectra at fiber lengths of 10 mm and 50 mm cover wavelength ranges from 2.4 μm to 4.6 μm and 1.7 μm to > 8.8 μm, producing a −40 dB bandwidth of 2200 nm and > 7100 nm (> 3.2 octaves), respectively. The corresponding spectral evolutions along the fiber length are shown in Fig. 3(b) and (c). It can be observed that the spectral evolution initially broadens because of SPM, visible after propagation lengths of 10 mm and 2 mm. Subsequently, FWM occurs, indicated by the spectral asymmetry in the wavelength domain (and symmetry in the frequency domain) [4], which becomes apparent after propagation lengths of 20 mm and 4 mm. The calculated nonlinear parameters for the two peak powers yield soliton fission lengths of $L_{fiss} = 26.3$ mm and 4.82 mm and soliton order of $N = 40$ and 7, respectively. These results indicate that the observed features arise from high-order soliton dynamics, where the pulse evolves into multiple short sub-pulses along the fiber. This is evident from the multiple intensity peaks (shown in dark yellow) in the temporal profiles at the soliton fission lengths in Fig. 3(e) and (f). The interaction of these soliton pulses causes an energy shift toward longer wavelengths. Consequently, the key nonlinear mechanisms driving SC generation are SPM, FWM, and soliton fission. The broadest SC spectra are observed at fiber lengths of approximately 26 mm and 4 mm, just before soliton fission occurs.

To investigate the influence of peak power and anomalous dispersion, we simulated SC generation in the three $AsSe_2$-As_2S_5 ChG HMOFs with $R = 4.4$ μm and $r = 1.9$, $R = 4.4$ μm and $r = 2.0$, and $R =$

4.4 µm and $r = 2.1$, using peak powers of 100, 500, 1000, 2000, and 3000 W, under identical pumping conditions. Their anomalous dispersions at the pump wavelength of 3.4 µm are $D = +4$ ps/nm/km, +8 ps/nm/km, and +12 ps/nm/km, respectively, as shown in Fig. 2(a). The resulting spectra of the widest SC generation are demonstrated, as seen in Fig. 4(a), (b), and (c), respectively. It is evident from the three figures that the widest SC spectra at the same peak power can be expanded equally, but the SC spectrum of each fiber occurs at different fiber lengths for each case. For the three fibers, the calculated parameters of soliton order (N) and soliton fission lengths (L_{fiss}) for the increasing peak powers were $N = 7$, 16, 23, 33, and 40 and $L_{\text{fiss}} = 26$, 11.8, 8.3, 5.9, and 4.8 mm; $N = 9$, 20, 29, 41, and 50 and $L_{\text{fiss}} = 35$, 16, 11, 8, and 6.5 mm; and $N = 14$, 33, 46, 66, and 81 and $L_{\text{fiss}} = 61$, 27.5, 19.5, 13.7, and 11.2 mm, respectively. These parameters indicate that the wider spectrum shifted from left to right with increasing peak power; the shift is due to nonlinear phenomena related to increasing the high-order soliton and decreasing the nonlinear length and the soliton fission length. In addition, the increased dispersion in the three fibers also results in the widest SC spectrum, occurring with increasing fiber length. At the highest peak power of 3000 W, the widest SC spectra can extend over wavelength ranges from 1.7 µm to 9.3 µm, 1.9 µm to 8.8 µm, and 1.8 µm to 9.2 µm, covering −40 dB bandwidths of 7600, 6900, and 8400 nm at propagation lengths of 4.0, 4.8, and 5.2 mm, respectively—values comparable to their soliton fission lengths. Therefore, the dominant nonlinear processes responsible for SC generation are SPM and FWM.

To examine the roles of pulse duration and pulse energy in SC generation, we repeated the simulations for the optimized $AsSe_2$-As_2S_5 ChG HMOF with $R = 4.4$ µm and $r = 1.9$ µm, using different pulse durations of $T_{\text{FWHM}} = 50$, 100, 200, and 300 fs at a peak power of 3000 W at the wavelength of 3.4 µm. The SC results are presented in Fig. 5. The widest SC spectra are obtained at fiber lengths of 1.2, 2.4, 4.0, and 5.8 mm, covering wavelength ranges from 1.8 µm to 8.2 µm, 1.7 µm to 9.1 µm, 1.7 µm to 9.3 µm, and 1.7 µm to 10.2 µm, corresponding to −40 dB bandwidths of 6400, 7400, 7600, and 8500 nm, respectively. The calculated soliton order and pulse energies are $N = 10$, 20, 40, and 61, corresponding to pulse energies of 0.92, 0.46, 0.23, and 0.15 pJ, with soliton fission lengths of 1.2, 2.4, 4.8, and 7.2 mm, respectively. Clearly, increasing T_{FWHM} leads to broader SC bandwidths because of higher pulse energy and soliton order; however, it also affects the flatness due to multiple short pulse propagations. As seen in Fig. 3(b), (c), (e), and (f), the spectral variations depend on the high-order soliton, and they can be reduced by selecting the optimized fiber length prior to soliton fission. The dominant physical mechanisms underlying SC formation are SPM and FWM.

CONCLUSION

We have numerically demonstrated ultra-broadband Mid-IR SC generation using the all-anomalous dispersion $AsSe_2$-As_2S_5 ChG HMOFs. The optimized $AsSe_2$-As_2S_5 ChG HMOF, consisting of an $AsSe_2$ ChG core with a radius of 1.9 µm and an As_2S_5 ChG cladding with a radius of 4.4 µm, exhibits all-anomalous dispersion with a small magnitude over the wavelength range from $\sim$ 3.2 µm to $>$ 10 µm, with ZDW of $\sim$ 3.3 µm. This fiber supports a well-confined fundamental TE mode over the wavelength range from $\sim$ 2 µm to 10 µm, using a 2D FDE solver. The nonlinear evolution within the fiber is simulated using SSFM. When pumped with 200-fs pulses at a wavelength of 3.4 µm with a peak power of 3000 W, the 4.0-mm-long fiber generated the widest SC spectrum, extending from 1.7 µm to 9.3 µm, with a −40 dB bandwidth of 7600 nm. This broadening resulted from strong nonlinear effects associated with the high nonlinear parameters of the fiber, dominated by SPM and FWM. Furthermore, by increasing the pulse duration to 300 fs with the same pump source, the 5.8-mm-long $AsSe_2$-As_2S_5 ChG HMOF produced an even broader SC spectrum, spanning from 1.7 µm to 10.2 µm, corresponding to a −40 dB bandwidth of 8500 nm ($>$ 1.1 octaves). This work highlights the novelty of the proposed $AsSe_2$-As_2S_5 ChG HMOF, which enables Mid-IR SC generation extending beyond 10 µm, using a compact and simply fabricated structure produced via the rod-in-tube drawing technique. The practical feasibility of the proposed Mid-IR SC device has been demonstrated, as As_2S_5 and $AsSe_2$ ChG materials and 200-fs pulses at 3.4 µm have been successfully employed to fabricate a four-hole $AsSe_2$-As_2S_5 HMOF. Combining ultra-broadband Mid-IR SC generation, a compact design, and low-energy ($<$ 1 pJ) pulses, this high-performance Mid-IR SC source shows strong potential for practical applications and scalable manufacturing.

Acknowledgements: The authors would like to extend their acknowledgments to Ramkhamhaeng University, Bangkok, Thailand, and Valaya Alongkorn Rajabhat University Demonstration School for their support.

REFERENCES

1. Dudley JM, Genty G, Coen S (2006) Supercontinuum generation in photonic crystal fiber. *Rev Mod Phys* **78**, 1135–1184.
2. Agrawal GP (2013) *Nonlinear Fiber Optics*, 5th edn, Academic, San Diego, California.
3. Petersen C, Prtljaga N, Farries M, Ward J, Napier B, Lloyd G, Nallala J, Stone N, et al (2018) Mid-infrared multispectral tissue imaging using a chalcogenide fiber supercontinuum source. *Opt Lett* **43**, 999–1002.
4. Lamont MRE, Luther-Davies B, Choi DY, Madden S, Eggleton BJ (2008) Supercontinuum generation in dispersion engineered highly nonlinear ($g = 10$ /W/m)

As_2S_3 chalcogenide planar waveguide. *Opt Express* **16**, 14938–14944.

5. Karim MR, Rahman BMA, Agrawal GP (2015) Mid-infrared supercontinuum generation using dispersion engineered $Ge_{11.5}As_{24}Se_{64.5}$ chalcogenide channel waveguide. *Opt Express* **23**, 6903–6914.
6. Travers JC, Frosz MH, Dudley JM (2010) Supercontinuum generation. In: Dudley JM, Taylor JR (eds) *Optical Fibers*, Cambridge University Press.
7. Voropaev V, Xie S, Donodin A, Batov D, Tarabrin M, Troles J, Lazarev VJ (2023) Octave-spanning supercontinuum generation in As_2S_3-silica hybrid waveguides pumped by thulium-doped fiber laser. *Lightwave Technol* **41**, 5116–5122.
8. Saenkwa B, Anusasananan P, Wannaprapa M, Chiangga S, Yupapin P, Sonasang S, Suwanarat S (2024) Nonlinear compression of mid-infrared supercontinuum generation in dispersion-engineered As_2S_5 chalcogenide ridge waveguide. *Opt Continuum* **3**, 636–648.
9. Hudson DD, Baudisch M, Werdehausen D, Eggleton BJ, Biegert J (2014) 1.9 octave supercontinuum generation in a As_2S_3 step-index fiber driven by Mid-IROPCPA. *Opt Lett* **39**, 5752–5755.
10. Gao W, Duan Z, Asano K, Cheng T, Deng D, Matsumoto M, Misumi T, Suzuki T, et al (2014) Mid-infrared supercontinuum generation in a four-hole As_2S_5 chalcogenide microstructured optical fiber. *Appl Phys B* **116**, 847–853.
11. Møller U, Yu Y, Kubat I, Petersen CR, Gai X, Brilland L, Mechin D, Caillaud C, et al (2015) Multi-milliwatt mid-infrared supercontinuum generation in a suspended core chalcogenide fiber. *Opt Express* **23**, 3282–3291.
12. Wang F, Zhou X, Zhang X, Yan X, Li S, Suzuki T, Ohishi Y, Cheng T (2021) Mid-infrared cascaded stimulated Raman scattering and flat supercontinuum generation in an As-S optical fiber pump at 2 μm. *Appl Opt* **60**, 6351–6356.
13. Qu Y, Sun W, Cao J, Chen H, Jia H (2021) Coherent ultrabroad orbital angular momentum supercontinuum generation in an $AsSe_2$-As_2S_5 microstructured fiber with all-normal dispersion. *Opt Commun* **497**, 127191.
14. Cheng TL, Kanou Y, Deng D, Xue X, Matsumoto M, Misumi T, Suzuki T, Ohishi Y (2014) Fabrication and characterization of a hybrid four-hole $AsSe_2$-As_2S_5 microstructured optical fiber with a large refractive index difference. *Opt Express* **22**, 13322–13329.
15. Cheng TL, Kanou Y, Deng D, Xue X, Matsumoto M, Misumi T, Suzuki T, Ohishi Y (2014) Mid-infrared supercontinuum generation in a novel $AsSe_2$-As_2S_5 hybrid microstructured optical fiber. *Opt Express* **22**, 23019–23025.
16. Nakatani A, Tong H, Matsumoto M, Sakai G, Suzuki T, Ohishi Y (2022) Transverse Anderson localization of mid-infrared light in a chalcogenide transversely disordered optical fiber. *Opt Express* **30**, 5159–5166.
17. Cordeiro CMB, Ng AKL, Ebendorff-Heidepriem H (2020) Ultra-simplified single-step fabrication of microstructured optical fiber. *Sci Rep* **10**, 9678.
18. Ma P, Choi DY, Yu Y, Gai X, Yang Z, Madden S, Luther-Davies B (2013) Low-loss chalcogenide waveguides for chemical sensing in the mid-infrared. *Opt Express* **21**, 29927–29937.
19. Salem AB, Diouf M, Cherif R, Wague A, Zghal M (2016) Ultraflat-top midinfrared coherent broadband supercontinuum using all normal As_2S_5-borosilicate hybrid photonic crystal fiber. *Opt Eng* **55**, 066109.
20. Diouf M, Ben Salem A, Cherif R, Wague A, Zghal M (2016) High power broadband Mid-infrared supercontinuum fiber laser using a novel chalcogenide $AsSe_2$ photonic crystal fiber. *Opt Materials* **55**, 10–16.
21. Tuniz A, Brawley G, Moss DJ, Eggleton BJ (2008) Two-photon absorption effects on Raman gain in single mode As_2Se_3 chalcogenide glass fiber. *Opt Express* **16**, 18524–18534.
22. Slusher RE, Lenz G, Hodelin J, Sanghera J, Shaw LB, Aggarwal ID (2004) Large Raman gain and nonlinear phase shifts in high-purity As_2Se_3 chalcogenide fibers. *J Opt Soc Am B* **21**, 1146–1155.
23. Fallahkhair AB, Li KS, Murphy TE (2008) Vector finite difference modesolver for anisotropic dielectric waveguides. *J Lightwave Technol* **26**, 1423–1431.
24. Murphy TE (2024) Software available at the Photonics Research Laboratory, University of Maryland. Available at: https://photonics.umd.edu/software/wgmodes.
25. Ansys Canada Ltd (2024) Waveguide FDE solver. Available at: https://optics.ansys.com/hc/en-us/articles/360042800453-Waveguide-FDE.
26. Yin L, Lin Q, Agrawal GP (2007) Soliton fission and supercontinuum generation in silicon waveguides. *Opt Lett* **32**, 391–393.
27. Travers JC, Frosz MH, Dudley JM (2010) *Supercontinuum Generation in Optical Fibers – Book Code (MATLAB Source Code Repository)*, GitHub. Available at: https://github.com/jtravs/SCGBookCode.
28. Fokoua ERN (2009) Ultrashort pulse propagation and supercontinuum generation in silicon-on-insulator optical nanowaveguides. ME Thesis, Universiteit Gent, Belgium.